Acta Crystallographica Section B
Structural Science
ISSN 0108-7681

Investigation of the structure and phase transitions of the polymeric inorganic–organic hybrids: $[M(\mathrm{Im})_4\mathrm{V}_2\mathrm{O}_6]_\infty$; M = Mn, Co, Ni, Im = imidazole

Kittipong Chainok,[a] Kenneth J. Haller,[a]* A. David Rae,[b] Anthony C. Willis[b] and Ian D. Williams[c]

[a]School of Chemistry, Institute of Science, Suranaree University of Technology, Nakhon Ratchasima 30000, Thailand, [b]Research School of Chemistry, Australian National University, Canberra, ACT 0200, Australia, and [c]Department of Chemistry, Hong Kong University of Science and Technology, Clear Water Bay, Kowloon, Hong Kong, People's Republic of China

Correspondence e-mail: ken.haller@gmail.com

Received 28 March 2010
Accepted 21 October 2010

The polymeric isomorphous hybrid inorganic–organic vanadium oxide compounds $[M(\mathrm{Im})_4\mathrm{V}_2\mathrm{O}_6]_\infty$, M = Mn, Co, Ni, Im = imidazole, were investigated at various temperatures between 100 and 295 K by single-crystal X-ray diffraction. The crystals all contain two-dimensional polymeric sheets packed perpendicular to **c*** and are 1:1 disordered in the space group $P4_2/n$ (Z = 8) at 295 K. The disordered phase is reversibly transformed to an $I4_1/a$ ordered phase (Z = 32) below 281 K for the Mn compound and below 175 K for the Co compound. Within a localized region of the $I4_1/a$ phase eight imidazoles are in close proximity and seven of these are hydrogen bonded to framework O atoms. The hydrogen-bond connectivity of six of these ligands is unchanged by the phase transition that allows an inversion of the local geometry using an inversion operator that is a symmetry element of $P4_2/n$, but not $I4_1/a$. The Mn structure has a well defined phase transition but the Co structure shows a large hysteresis and it was necessary to include stacking faults in the modelling of the Co structure at low temperatures. The Ni structure was shown to be partially twinned, but ordered in the space group $P2/n$ (Z = 8) at 100 K, with two different localized regions each containing four pairs of inversion-related imidazoles, hydrogen bonding to framework O atoms involving eight imidazoles in one region and six imidazoles in the other. Models for the phase transition mechanisms are considered.

1. Introduction

Open framework materials based on inorganic–organic hybrids involving metal oxides and organic templates are of great contemporary interest in the fields of materials science and chemical research (Natarajan & Mandal, 2008). They have a topological diversity with a rich variety of structure types and bonding geometries (Cheetham *et al.*, 1999; O'Keeffe *et al.*, 2008) that allows potential applications in the fields of catalysis, magnetism, photochemistry and sorption (Lin *et al.*, 2009; Maspoch *et al.*, 2007; Xie *et al.*, 2010). In the last few years, polymers of such hybrids, particularly those involving vanadium oxide and a secondary transition metal have been made using a hydrothermal approach with an aliphatic amine as a template that provides space filling or charge compensation and thus acts as a structure-directing agent (Chirayil *et al.*, 1998; Chesnut *et al.*, 1999; Hagrman *et al.*, 2001).

Many of these compounds are frameworks built from edge and corner sharing of VO_4 tetrahedra, square VO_5 pyramids or VO_6 octahedra (Zavalij & Whittingham, 1999) along with

other metal polyhedra. They have been investigated with possible applications as secondary cathode materials (Höwing *et al.*, 2003; Whittingham, 2004) and as chiral materials (Krachodnok *et al.*, 2008). Many hybrid inorganic–organic vanadium oxide structures have been determined by single-crystal X-ray diffraction. A search of the Cambridge Structure Database shows that despite many of these materials displaying disorder that effects the resulting physical properties, the structures have usually only been evaluated at room temperature. Temperature-induced phase transitions are of great importance in solid-state chemistry (Herbstein, 2006) and an investigation into the temperature dependence of a structure can reveal much about how structure variation affects physical properties.

The present work forms part of an exploration of inorganic–organic hybrids involving vanadium oxide. One focus of this research is to use the aromatic diamine planar geometry of imidazole and hydrothermal syntheses to introduce secondary inorganic metal sites. This molecule is different from the aliphatic diamines previously used (Law *et al.*, 2000; Law & Williams, 2000; Williams *et al.*, 2000) in terms of basicity, size, shape, ligation ability, hydrogen-bond capacity and charge, and this could allow different and more diverse framework structures.

In this paper we report the single-crystal structures and temperature dependence of three new isomorphous inorganic–organic hybrid vanadium oxide compounds with the formula $[M(\mathrm{Im})_4\mathrm{V_2O_6}]_\infty$ [M = Mn in (I), Co in (II), Ni in (III) and Im = imidazole]. The crystal structures consist of two-dimensional polymeric sheets packed perpendicular to the **c*** direction. Each $M\mathrm{N_4O_2}$ octahedron involves four separate imidazoles and two separate $\mathrm{VO_4}$ tetrahedra. Each $\mathrm{VO_4}$ tetrahedron shares one oxygen with an M atom and two O atoms with separate $\mathrm{VO_4}$ tetrahedra, the remaining oxygen being terminal. The crystals each show a reversible order–disorder phase change. The low-temperature phase has the space group $I4_1/a$ [(I) and (II)] or $P2/n$ (III), while the high-temperature phase has the space group $P4_2/n$. The high-temperature phase exists at 298 K and can be regarded as a disordering of the low-temperature phases (*i.e.* the low-temperature space groups correspond to different orderings of the 1:1 disordered $P4_2/n$ structure. We have studied the M = Mn structures 2 K above and 2 K below the transition temperature as well as at other temperatures to improve our understanding of the changes in bonding with temperature for these compounds. The M = Co structures were similarly investigated but a $\pm$ 5 K interval about the phase transition was used. The asymmetric unit for the $P4_2/n$ structure is related to the asymmetric unit of the $I4_1/a$ structure by the fractional coordinate transformation $x_\mathrm{P} = x_\mathrm{I} + y_\mathrm{I} - 1$, $y_\mathrm{P} = -x_\mathrm{I} + y_\mathrm{I} + 1$, $z_\mathrm{P} = 2z_\mathrm{I}$ corresponding to the cell transformation $\mathbf{a}_\mathrm{P} = 1/2(\mathbf{a}_\mathrm{I} + \mathbf{b}_\mathrm{I})$, $\mathbf{b}_\mathrm{P} = \frac{1}{2}(-\mathbf{a}_\mathrm{I} + \mathbf{b}_\mathrm{I})$, $\mathbf{c}_\mathrm{P} = 2\mathbf{c}_\mathrm{I}$. The M = Ni structure was investigated at 100 and 295 K only. The low-temperature structure has the space group $P2/n$ and has coordinates for the asymmetric unit related to the $P4_2/n$ structure by the transformation $x = x_\mathrm{p}$, $y = z_\mathrm{p}$, $z = y_\mathrm{p}$ corresponding to the cell transformation $\mathbf{a} = -\mathbf{a}_\mathrm{p}$, $\mathbf{b} = -\mathbf{c}_\mathrm{p}$, $\mathbf{c} = -\mathbf{b}_\mathrm{p}$.

2. Experimental

2.1. Hydrothermal synthesis

Mixtures of the vanadium pentoxide precursor, manganese, cobalt or nickel acetate, imidazole and distilled water in the molar ratio 1:1:11.8:444 gave good highly crystalline yields of isomorphous compounds with similar morphology (hexagonal-shaped single crystals, often inter-grown, with a diameter up to 2.5 mm and thickness in the range 0.05–1.0 mm). The temperature of the reaction is of crucial importance for the crystallization of M/V/O/imidazole products. Experiments conducted at temperatures of 413 K or higher gave black–brown powders that do not contain imidazole, as verified by FTIR studies. These materials were not characterized further. However, maintaining the reaction temperature between 383 and 393 K generally gave two products, a major crystalline material and a residual powder. Reactions of vanadium oxide with a secondary metal in the presence of imidazole were therefore generally controlled near 393 K to produce good crystalline products. Time also affected the morphology and particle size of the crystallized products. To grow single crystals with the dimensions 0.2–0.4 mm suitable for X-ray crystallography required typical reaction times of 4–5 d. The balanced chemical equations representing the syntheses of the crystalline product need not correspond to the actual stoichiometric ratio of reactants required to maximize the crystalline product yield, since other products are also formed. There are at least five factors that influence the composition and structure of the reaction products: stoichiometry, temperature, reaction time, concentration and pH. The conditions reported below appear to be optimum for preparing the structures reported here in highly crystalline form. The compounds are phase pure by microscopic examination, microelemental analysis and powder X-ray diffraction. The room-temperature PXRD patterns of bulk materials of (I), (II) and (III) are in good agreement with those calculated from the single-crystal data.

A typical procedure to make (I), $[\mathrm{Mn(Im)_4V_2O_6}]_\infty$, was to mix $\mathrm{V_2O_5}$ (0.18 g, 1.0 mmol), $\mathrm{Mn(OAc)_2{\cdot}4H_2O}$ (0.25 g, 1.0 mmol), Im (0.8 g, 11.8 mmol), in distilled water (5 ml, 277.5 mmol) and stir for 2 h in air to form an orange–yellow mixture, which was placed in a Teflon container, sealed in a 23 ml Parr reactor, placed in an oven, and heated from room temperature to 393 K under autogenous pressure for 5 d. After cooling, the product was filtered off from the bright yellow mother liquor, washed with distilled water and then dried overnight at room temperature. Orange–yellow block-shaped crystals were easy to separate from a residual uncharacterized yellow–brown powder by hand under an optical microscope. The yield was 90% (0.14 g) based on $\mathrm{V_2O_5}$. Anal.: found (calc.) for $\mathrm{C_{12}H_{16}MnN_8O_6V_2}$: C 27.43 (27.45); H 2.98 (3.07); N 21.37 (21.34)%. EDX; V:Mn = 2:1. IR (KBr, $\mathrm{cm^{-1}}$): 3430(w), 3126(w), 3048(w), 2942(w), 2840(w), 1536(m), 1492(w), 1480(w), 1431(m), 1327(m), 1262(w), 1094(m), 1065(s), 927(s), 790(s), 655(s), 614(m), 547(m). TGA (under $\mathrm{N_2}$, rate 5 K $\mathrm{min^{-1}}$) $-\Delta w$ (423–923 K) = 52.1%,

corresponding to a loss of imidazole molecules (51.9% theory).

The Co [(II)] and Ni [(III)] analogues were obtained similarly using cobalt(II) or nickel(II) acetate tetrahydrate as cobalt or nickel sources.

$[Co(Im)_4V_2O_6]_\infty$ (II): Orange–red block-shaped crystals were easy to separate from a residual uncharacterized purple powder by hand under an optical microscope. The yield was 95% (0.15 g) based on V_2O_5. Anal. found (calc.) for $C_{12}H_{16}CoN_8O_6V_2$: C 27.41 (27.19)%; H 2.92 (3.04)%; N 21.16 (21.14)%. EDX; V:Co = 2:1. IR (KBr, cm^{-1}): 3401(w), 3122(w), 3042(w), 2935(w), 2836(w), 1534(m), 1490(w), 1479(w), 1427(m), 1326(m), 1262(w), 1091(m), 1065(s), 925(s), 788(s), 654(s), 612(m), 546(m). TGA (under N_2, rate 5 K min^{-1}) $-\Delta w$ (448–903 K) = 52.0%, corresponding to a loss of imidazole molecules (51.5% theory).

$[Ni(Im)_4V_2O_6]_\infty$ (III): Blue block-shaped crystals were easy to separate from a residual uncharacterized brown–blue powder by hand under an optical microscope. The yield was 90% (0.14 g) based on V_2O_5. Anal. found (calc.) for $C_{12}H_{16}NiN_8O_6V_2$: C 26.97 (27.25)%; H 2.97 (3.05)%; N 21.07 (21.19)%. EDX; V:Ni = 2:1. IR (KBr, cm^{-1}): 3991(w), 3118(w), 3039(w), 2931(w), 2834(w), 1533(m), 1488(w), 1473(w), 1425(m), 1324(m), 1262(w), 1089(m), 1065(s), 924(s), 787(s), 654(s), 611(m), 541(m). TGA (under N_2, rate 5 K min^{-1}) $-\Delta w$ (453–898 K) = 51.9%, corresponding to a loss of imidazole molecules (51.5% theory).

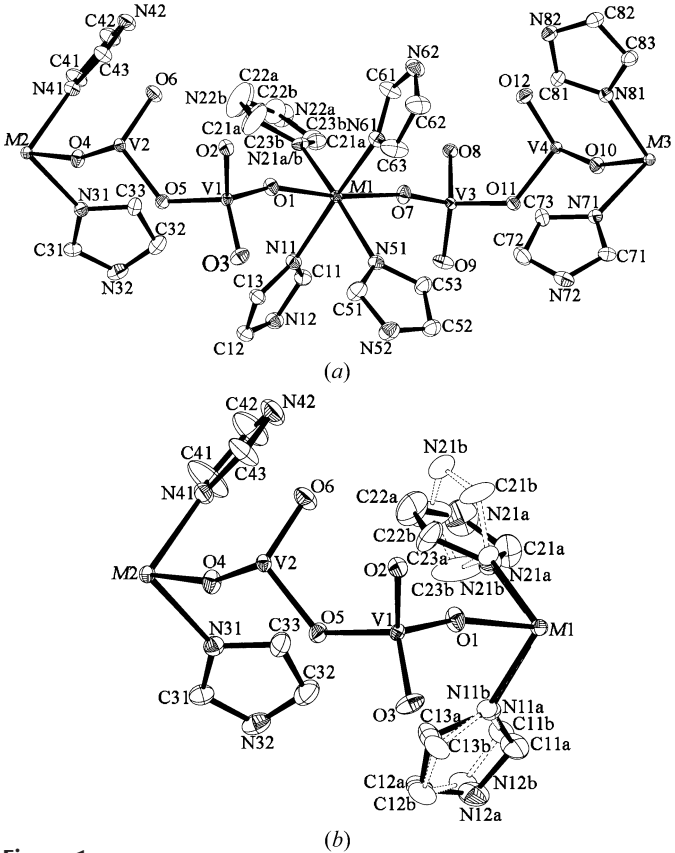

Figure 1
The asymmetric unit of (*a*) the $I4_1/a$ structure (at 100 K) and (*b*) the $P4_2/n$ structure (at 295 K) of (I) viewed down equivalent directions with 50 and 25% displacement ellipsoids. The environment on the right of the twofold axis in Fig. 1(*a*) transforms to the environment as depicted on the left of the axis. H atoms are omitted for clarity.

2.2. X-ray crystallography

2.2.1. Data collection. Single crystals with dimensions 0.16 × 0.14 × 0.09 mm (I), 0.25 × 0.19 × 0.18 mm (II), and 0.40 × 0.21 × 0.18 mm (III) were used. Reflection intensities were collected on an Enraf–Nonius KappaCCD four-circle area-detector diffractometer using the *COLLECT* (Nonius, 1998) software. The diffractometer was equipped with a graphite monochromator, a 0.3 mm *ifg* capillary collimator and a fine-focus X-ray tube with Mo $K\alpha$ radiation, λ = 0.71073 Å. The sample-to-detector distance was 35.0 mm. The frame images were reduced to intensity data using the *DENZO* and *SCALEPACK* software (Otwinowski & Minor, 1997). A numerical absorption correction by the multiscan method was applied (Blessing, 1995).

Diffraction data sets were collected using the same crystal at different temperatures for each compound: 100, 200, 279, 283 and 295 K for (I), 100, 170, 180 and 295 K for (II), and 100 and 295 K for (III). An Oxford Cryosystems (1997) 600 cooling device was used. Temperatures were approached *via* slow cooling over a 1 h period and annealing for 10 min at each temperature before data collection commenced.

2.2.2. Structure solution and refinement. Structures were solved by direct methods using *SIR*97 (Altomare *et al.*, 1999) and expanded using Fourier techniques. Atomic scattering factors and anomalous dispersion parameters were from the *International Tables for X-ray Crystallography*, Vol. C (Creagh & McAuley, 1995). The structures were refined by full matrix refinement on *F* using *RAELS*06 (Rae, 2006). The same parameterization model was used for each temperature of a particular phase.

Refinement of the low-temperature $I4_1/a$ phase used origin choice 2 of the *International Tables for X-ray Crystallography*, Vol. A (Hahn, 1995*a*,*b*), and 317 variables to describe 64 non-H and 36 H-atom positions. A separate scale constant for reflections with *l* odd was added for the Co structure. The second of eight imidazoles in the asymmetric unit (see Fig. 1*a*) was found to be disordered. All H atoms were reinserted in geometrically sensible positions after each refinement cycle and given atomic displacement parameters defined by the 12 variable *TL* rigid-body model (Rae, 1975*a*,*b*) that described the anisotropic atomic displacement parameters of the corresponding imidazole (or disordered imidazole). The centers of action for the librations were located on the associated *M* atom. A common set of refinable local orthonormal coordinates were used to impose equal planar geometry on every imidazole, their origins and orientations being independently determined. The twofold rotation-related components of the disordered imidazole were constrained to be coplanar with the coordinating N atoms coincident. The metal and oxygen atoms were refined as independent anisotropic atoms. Atoms *M*2 and *M*3 lie on a twofold axes.

Table 1
Experimental details of (I) at selected temperatures.

Experiments were carried out with Mo $K\alpha$ radiation using an Enraf–Nonius KappaCCD diffractometer. H-atom parameters were constrained. A numerical absorption correction by the multiscan method from symmetry-related measurements, *SORTAV* (Blessing, 1995), was applied.

	100 K	200 K	279 K	283 K	295 K
Crystal data					
Chemical formula	$[Mn(C_3H_4N_2)_4V_2O_6]$	$[Mn(C_3H_4N_2)_4V_2O_6]$	$[Mn(C_3H_4N_2)_4V_2O_6]$	$[Mn(C_3H_4N_2)_4V_2O_6]$	$[Mn(C_3H_4N_2)_4V_2O_6]$
M_r	525.13	525.13	525.13	525.13	525.13
Cell setting, space group	Tetragonal, $I4_1/a$	Tetragonal, $I4_1/a$	Tetragonal, $I4_1/a$	Tetragonal, $P4_2/n$	Tetragonal, $P4_2/n$
a, c (Å)	23.0354 (3), 29.6005 (3)	23.0473 (3), 29.6521 (3)	23.0645 (3), 29.6897 (3)	16.3271 (2), 14.8304 (2)	16.3615 (2), 14.8030 (2)
V (Å^3)	15 706.9 (3)	15 750.5 (3)	15 794.1 (3)	3953.40 (9)	3962.74 (9)
Z	32	32	32	8	8
μ (mm^{-1})	1.61	1.61	1.61	1.61	1.61
Crystal size (mm)	0.16 × 0.14 × 0.09	0.16 × 0.14 × 0.09	0.16 × 0.14 × 0.09	0.16 × 0.14 × 0.09	0.16 × 0.14 × 0.09
Data collection					
Absorption correction	Multi-scan	Multi-scan	Multi-scan	Multi-scan	Multi-scan
T_{min}, T_{max}	0.684, 0.767	0.708, 0.768	0.707, 0.765	0.678, 0.765	0.672, 0.765
No. of measured, independent and observed $[I > 3\sigma(I)]$ reflections	106 159, 11 464, 8019	96 520, 11 499, 7205	109 552, 11 539, 6608	55 800, 5769, 4293	54 609, 5784, 4271
R_{int}	0.058	0.061	0.059	0.055	0.059
Refinement					
$R[F^2 > 3\sigma(F^2)]$, $wR(F^2)$, S	0.032, 0.046, 1.47	0.033, 0.046, 1.45	0.035, 0.050, 1.56	0.048, 0.075, 2.59	0.040, 0.060, 2.06
No. of reflections	8019	7205	6608	4293	4271
No. of parameters	317	317	317	174	174
No. of restraints	2	2	2	6	6
$(\Delta/\sigma)_{max}$	0.2	0.2	0.2	0.2	0.2
$\Delta\rho_{max}$, $\Delta\rho_{min}$ (e Å^{-3})	1.22, −0.98	0.76, −0.70	1.08, −0.70	2.14, −1.24	1.11, −0.80

Computer programs used: *COLLECT* (Nonius, 1997), *HKL SCALEPACK*, *DENZO*, *SCALEPAK* (Otwinowski & Minor, 1997), *SIR*97 (Altomare *et al.*, 1999), *RAELS*06 (Rae, 2006), *ORTEP* (Burnett & Johnson, 1996), *DIAMOND* (Brandenburg & Putz, 2006).

Refinement of the high-temperature $P4_2/n$ phases used origin choice 2 (Hahn, 1995*a*,*b*), and 174 variables to describe 40 non-H- and 24 H-atom positions. The first and second of the four imidazoles in the asymmetric unit (see Fig. 1*b*) were described as 1:1 disordered and given labels 1*a* and 1*b*, and 2*a* and 2*b*. All other atoms were modelled as being ordered. All H atoms were reinserted in geometrically sensible positions after each refinement cycle and given atomic displacement parameters defined by the rigid-body models for the atoms to which they were attached. The two disordered imidazoles are attached to the *M*1 atom and their atoms were modelled to have a common *T* rigid model parameterization plus individual librations about the relevant *M*1—N bonds (Rae, 1975*b*). The other two imidazoles were attached to *M*2 and were also modelled to have a common *T* rigid model parameterization plus individual librations about the relevant *M*2—N bonds. A common set of refinable local orthonormal coordinates was used to impose equal planar geometry on every imidazole, their origins and orientations being independently determined. Restraints were used to match the *M*1—N bond distances of each component of a disordered imidazole. Restraints were also used to initially restrain second nearest-neighbor *M*1—C distances, but these restraints were reduced to minimal importance in the final refinement cycle. The metal atoms and oxygen atoms were refined as independent anisotropic atoms. Atoms *M*1 and *M*2 lie on twofold axes.

For *M* = Ni (III), the low-temperature $P2/n$ phase used 287 variables to describe 60 non-H- and 32 H-atom positions in the asymmetric unit. Only the sixth of eight imidazoles is not hydrogen bonded and a mixed scattering factor description was used to account for the disorder of N62 and C62, modeled for C62 as $(1 - \delta_1)f_C + \delta_1 f_N$ and N62 as $(1 - \delta_2)f_C + \delta_2 f_N$, where $\delta_1 + \delta_2 = 1$ gave $\delta_1 = 0.035$ (25). All H atoms were reinserted in geometrically sensible positions after each refinement cycle and given atomic displacement parameters defined by the rigid-body models applying to the atoms to which they were attached. In the asymmetric unit, pairs of imidazoles are attached to non-equivalent Ni atoms on twofold axes and were given rigid-body *T* model parameters constrained by this symmetry (Rae, 1975*a*,*b*). Additional *L* model (Rae, 1975*b*) parameters (six per imidazole) centered on the relevant Ni were also included to describe the imidazole atom displacement parameters by 4 × (4 + 2 × 6) = 64 variables. A common set of refinable local orthonormal coordinates were used to impose equal planar geometry on the imidazoles, their origins and orientations being independently refined. No restraints were used. The metal and oxygen atoms were refined as independent anisotropic atoms. The crystals were found to be 0.746 (3):0.254 twinned assuming a 90° rotation about **b** as the twinning operation and allowing for the overlap of adjacent reflections modeling the observed intensity using the function $Y = 0.746|F_1|^2 + 0.254P|F_2|^2$, where $P = 0.5 - 0.5\sin(\pi(d - d_o)/$

Table 2
Experimental details of (II) at selected temperature.

Experiments were carried out with Mo $K\alpha$ radiation using an Enraf–Nonius KappaCCD diffractometer. H-atom parameters were constrained. A numerical absorption correction by the multiscan method from symmetry-related measurements, *SORTAV* (Blessing, 1995), was applied.

	100 K	170 K	180 K	295 K
Crystal data				
Chemical formula	$[Co(C_3H_4N_2)_4V_2O_6]$	$[Co(C_3H_4N_2)_4V_2O_6]$	$[Co(C_3H_4N_2)_4V_2O_6]$	$[Co(C_3H_4N_2)_4V_2O_6]$
M_r	529.13	529.13	529.13	529.13
Cell setting, space group	Tetragonal, $I4_1/a$	Tetragonal, $I4_1/a$	Tetragonal, $P4_1/n$	Tetragonal, $P4_2/n$
a, c (Å)	22.8606 (3), 29.2658 (3)	22.8863 (3), 29.2700 (3)	16.2544 (2), 14.5532 (2)	16.2666 (3), 14.6057 (2)
V (Å^3)	15 294.5 (3)	15331.1 (3)	3845.1 (1)	3864.7 (1)
Z	32	32	8	8
μ (mm^{-1})	1.86	1.86	1.86	1.86
Crystal size (mm)	0.25 × 0.19 × 0.18	0.25 × 0.19 × 0.18	0.25 × 0.19 × 0.18	0.25 × 0.19 × 0.18
Data collection				
Absorption correction	Multi-scan	Multi-scan	Multi-scan	Multi-scan
T_{min}, T_{max}	0.636, 0.720	0.639, 0.719	0.658, 0.721	0.662, 0.720
No. of measured, independent and observed [$I > 3\sigma(I)$] reflections	127 079, 11 163, 7414	107 994, 11 199, 6461	59 858, 5608, 4475	57 596, 5657, 3905
R_{int}	0.059	0.057	0.046	0.059
Refinement				
$R[F^2 > 3\sigma(F^2)]$, $wR(F^2)$, S	0.035, 0.056, 1.85	0.040, 0.065, 2.10	0.032, 0.050, 1.81	0.033, 0.047, 1.56
No. of reflections	7414	6461	4475	3905
No. of parameters	318	318	174	174
No. of restraints	2	2	6	6
$(\Delta/\sigma)_{max}$	0.2	0.2	0.2	0.2
$\Delta\rho_{max}$, $\Delta\rho_{min}$ (e Å^{-3})	1.20, −1.13	2.40, −1.40	1.07, −0.53	0.72, −0.55

$2d_o$) if $d < 2d_o$, 0 otherwise. d is the separation in reciprocal space of overlapping twin component reflections and d_o was refined to be 0.1397 (5)a^*.

3. Results and discussion

The data collection and structure refinement details for (I), (II) and (III) at selected temperatures are listed in Tables 1, 2 and 3. Detailed refinement statistics are given in Table 4. The largest principal libration tensors for the imidazoles of the low- and high-temperature phases are summarized in Tables 5 and 6. Angles between normals to planes of pseudo-symmetry-related imidazoles for the low- and high-temperature phases are given in Tables 7 and 8. Selected bond lengths at 100 K for the compounds are listed in Tables 9 and 10. The hydrogen bonding at 100 and 295 K is described in Tables 11 and 12. The bond lengths and angles, hydrogen-bond geometry and other crystallographic data at all experiment temperatures are given as supplementary material.[1]

3.1. Description of the $I4_1/a$ phase

Compounds $C_{12}H_{16}MN_8O_6V_2$, M = Mn (I), Co (II), Ni (III), have isomorphous structures. The room-temperature structure (Z = 8) in the space group $P4_2/n$ (No. 86) is reversibly transformed to a body-centered structure (Z = 32) in the space group $I4_1/a$ (No. 88) at 281 K for (I) and 175 K for (II). The asymmetric unit along with the atomic numbering for the $I4_1/a$ structures are shown in Fig. 1(*a*). This figure is drawn for (I) down a direction 10° away from **a** + **b** with **c** vertical. In the $P4_2/n$ phase the two halves of the asymmetric unit become related by a twofold rotation axis parallel to **c** and passing through *M*1. Four crystallographically independent VO_4 tetrahedra are in general positions. Atoms *M*2 and *M*3 lie on twofold rotation axes that contain $\bar{4}$ sites. Atom *M*1 lies approximately on a 4_1 screw axis that corresponds to a 4_2 axis in the $P4_2/n$ structure. There are eight imidazole groups, seven of which are involved in hydrogen bonding. The imidazole labeled with a 2 is not hydrogen bonded, and is disordered with occupancy ratios that refined to (I): 0.776 (11):0.224 at 100 K, 0.698 (12):0.302 at 200 K, 0.618 (13):0.382 at 279 K, and (II): 0.425 (15):0.575 at 100 K, 0.389 (18):0.611 at 170 K.

The coordination polyhedra observed for the four V atoms exhibit distorted $[VO_4]$ tetrahedral coordination geometry with three μ_2-O atoms and a terminal O atom. The bond-valence sums (Brown & Altermatt, 1985; Brese & O'Keeffe, 1991) indicate that all the vanadiums are pentavalent. Each vanadium tetrahedron is connected *via* μ_2-O atoms. The pair (V1 and V2), likewise (V3 and V4), are mutually linked together through corner-shared μ_2-O atoms (O2 and O5), likewise (O8 and O11) to form $[V_4O_{12}]^{4-}$ tetranuclear rings about a center of inversion. This anionic cluster of $[V_4O_{12}]^{4-}$ resembles the prototypical structure observed in $(Bu_4N)_3HV_4O_{12}$ (Fuchs *et al.*, 1976) and $[PPh_4]_2V_4O_{11}$ (Sharma *et al.*, 2002). The O3, O6, O9 and O12 atoms are terminal. The remaining O atoms of O1, O4, O7 and O10 connect the relevant VO_4 tetrahedron to an *M* atom that displays a distorted octahedral geometry coordinated through nitrogen donors from four imidazole groups atoms in an

[1] Supplementary data for this paper are available from the IUCr electronic archives (Reference: GW5007). Services for accessing these data are described at the back of the journal.

Table 3
Experimental details of (III) at selected temperature.

Experiments were carried out with Mo $K\alpha$ radiation using an Enraf–Nonius KappaCCD diffractometer. H-atom parameters were constrained. A numerical absorption correction by the multiscan method from symmetry-related measurements, *SORTAV* (Blessing, 1995), was applied.

	100 K	295 K
Crystal data		
Chemical formula	$[Ni(C_3H_4N_2)_4V_2O_6]$	$[Ni(C_3H_4N_2)_4V_2O_6]$
M_r	528.90	528.90
Cell setting, space group	Monoclinic, $P2/n$	Tetragonal, $P4_2/n$
a, b, c (Å)	16.1379 (3), 14.3657 (2), 16.3422 (4)	16.1988 (2), 16.1988 (2), 14.5589 (2)
β (°)	90.1205 (9)	90
V (Å^3)	3788.64 (13)	3820.27 (8)
Z	8	8
μ (mm^{-1})	2.0	2.0
Crystal size (mm)	0.40 × 0.21 × 0.18	0.40 × 0.21 × 0.18
Data collection		
Absorption correction	Multi-scan	Multi-scan
T_{min}, T_{max}	0.619, 0.712	0.630, 0.703
No. of measured, independent and observed [$I > 3\sigma(I)$] reflections	53 813, 11 073, 9089	48 877, 5581, 4334
R_{int}	0.055	0.047
Refinement		
$R[F^2 > 3\sigma(F^2)]$, $wR(F^2)$, S	0.039, 0.053, 1.67	0.031, 0.048, 1.70
No. of reflections	9089	4334
No. of parameters	287	174
No. of restraints	0	6
$(\Delta/\sigma)_{max}$	0.2	0.2
$\Delta\rho_{max}$, $\Delta\rho_{min}$ (e Å^{-3})	2.30, −2.32	0.81, −0.65

equatorial plane and two O atoms from the anionic $[V_4O_{12}]$ clusters in axial positions. The metal atoms are not coplanar with respect to the imidazoles and this presumably is to satisfy packing and hydrogen-bonding demands.

Fig. 2(*a*) shows a single layer of the $I4_1/a$ structure at $z = \frac{1}{2}$ projected down the **c** axis. The framework consists of cyclic V_4O_{12} tetramers interconnected by MN_4O_2 octahedra. The framework topology is defined by two cyclic submotifs, namely, four corner-connected VO_4 tetrahedra forming eight-membered $\{V_4O_4\}$ small rings, and the four MN_4O_2 octahedra and eight VO_4 tetrahedra further connected to form 24-membered $\{M_4V_8O_{12}\}$ large rings. The 4_1 screw axis causes the centers of the small and large rings to alternate along the **c** direction with 1/4**c** spacing (*ca* 7.4 Å). Eight imidazoles connected to four different M atoms fill cavities centered on pseudo-inversion centers. Figs. 3(*a*) and (*b*) show the environment about such a site at $\frac{3}{4}, \frac{1}{4}, \frac{1}{2}$. The pseudo-inversion relates imidazoles equivalent to those labeled 1, 2, 3, and 4 to those labeled 5, 6, 7, and 8, respectively. The available hydrogen attached to the non-metal-coordinated nitrogen of the imidazole is involved in hydrogen bonding to an O atom for all imidazoles except that labeled 2. The bond connectivity is centrosymmetric for all the imidazoles except those labeled 2 and 6. The hydrogen bonds are of similar length (*ca* 2.8 Å) and connect N12, N32, N42, N52, N62, N72 and N82 to O12, O11, O3, O6, O9, O5 and O9, respectively. However, only the orientations of the imidazoles labeled 3 and 7 maintained a reasonably exact inversion relationship.

3.2. Description of the $P4_2/n$ phase

The high-temperature phase crystallizes in the space group $P4_2/n$ (No. 86), with eight formula units per unit cell. The asymmetric unit is illustrated in Fig. 1(*b*) for (I), and is related to the asymmetric unit of the $I4_1/a$ phase by the transformation $x_P = x_I + y_I - 1$, $y_P = -x_I + y_I + 1$, $z_P = 2z_I$ and occupies half the volume. This corresponds to relating two axial systems with a common origin so that $\mathbf{a}_P = \frac{1}{2}(\mathbf{a}_I + \mathbf{b}_I)$, $\mathbf{b}_P = \frac{1}{2}(-\mathbf{a}_I + \mathbf{b}_I)$, $\mathbf{c}_P = \frac{1}{2}\mathbf{c}_I$. Figs. 1(*a*) and (*b*) are drawn down the same direction. What was a 4_1 screw axis passing approximately through $M1$ is now a 4_2 screw axis containing a twofold rotation that relates two asymmetric units. Atoms $M1$ and $M2$ both lie on twofold axes. $M2$ is on an axis containing $\bar{4}$ sites. The coordination geometry around the metal centers is identical to the low-temperature $I4_1/a$ phase. The imidazoles 1 and 2 attached to $M1$ were each disordered over two positions, whereas this was found to be unnecessary for imidazoles 3 and 4 attached to $M2$. Again the metal atoms were not constrained to lie in the plane of the attached imidazoles. The occupancy refinement suggested ratios of 1:1 which were subsequently fixed.

The hydrogen-bond connectivity is equivalent to the $I4_1/a$ phase if one simply imposes exact inversion in the center of the cavity containing eight imidazole ligands as required by space group $P4_2/n$. Figs. 3(*c*) and (*d*) show the environment of the cavity at 0, $\frac{1}{2}$, 1, after ordering across the inversion center to best approximate the $I4_1/a$ phase, imidazoles 1–8 of the $I4_1/a$ phase corresponding to imidazoles 1*b*, 2*a*, 3, 4, 1*a*, 2*b*, 3, 4 of the $P4_2/n$ phase. It is seen that the major difference between the two phases is that imidazoles 4 and 8 that were not inversion equivalent in the $I4_1/a$ phase have joined imidazoles 3 and 7 in becoming inversion related in the $P4_2/n$ phase. To switch between inversion-related descriptions of the cavity only requires a change in the hydrogen-bond connectivity for imidazoles 2 and 6, two becoming hydrogen bonded and six losing their hydrogen bonds. The other changes simply involve reorienting the imidazoles without a change of hydrogen-bond connectivity.

The description of the $P4_2/n$ phase has departed from the model implied by disordering the $I4_1/a$ structure so as to ensure each refinement above the transition temperature was well behaved. We have ignored the inherent coplanar disorder

Table 4
Refinement statistics for (I), (II) and (III) at selected temperatures.

Temperature (K)	Class	No. of reflections	$R(F)$	$R(F^2)$	$wR(F)$	S
(I) at 100	1	4749	0.027	0.039	0.044	1.56
	2	3540	0.054	0.080	0.063	1.61
	1 + 2	8289	0.033	0.042	0.050	1.58
	1 + 2 + 3	11 464	0.055	0.046	0.057	1.53
(I) at 200	1	4515	0.028	0.041	0.043	1.49
	2	2914	0.059	0.089	0.063	1.54
	1 + 2	7429	0.034	0.044	0.049	1.51
	1 + 2 + 3	11 499	0.065	0.050	0.058	1.44
(I) at 279	1	4432	0.030	0.043	0.045	1.55
	2	2436	0.071	0.108	0.076	1.72
	1 + 2	6868	0.037	0.046	0.053	1.64
	1 + 2 + 3	11 539	0.080	0.053	0.065	1.56
(I) at 283	1	4397	0.049	0.064	0.076	2.61
	1 + 3	5769	0.065	0.067	0.079	2.38
(I) at 295	1	4352	0.041	0.068	0.060	2.06
	1 + 3	5784	0.058	0.071	0.065	1.92
(II) at 100	1	4687	0.028	0.040	0.047	1.77
	2	3186	0.092	0.125	0.109	2.46
	1 + 2	7873	0.040	0.044	0.065	2.08
	1 + 2 + 3	11 163	0.066	0.048	0.073	1.96
(II) at 170	1	4592	0.033	0.047	0.054	1.98
	2	2411	0.146	0.210	0.161	2.94
	1 + 2	7003	0.047	0.051	0.075	2.36
	1 + 2 + 3	11 199	0.085	0.057	0.086	2.13
(II) at 180	1	4450	0.032	0.044	0.051	1.84
	1 + 3	5608	0.043	0.046	0.054	1.77
(II) at 295	1	3990	0.034	0.045	0.048	1.60
	1 + 3	5657	0.059	0.050	0.056	1.55
(III) at 100	1	9244	0.040	0.059	0.054	1.70
	1 + 3	11 073	0.049	0.061	0.056	1.62
(III) at 295	1	4420	0.032	0.044	0.049	1.73
	1 + 3	5581	0.044	0.046	0.053	1.66

Class 1: reflection with $I > 3\sigma(I)$ and $h + k + l$ even. Class 2: reflection with $I > 3\sigma(I)$ and $h + k + l$ odd. Class 3: reflection all with $I < 3\sigma(I)$ and not included in the refinement. Average of F^2 for Class 2 relative to Class 1 is 0.111 (100 K), 0.098 (200 K), and 0.082 (279 K) for (I), 0.066 (100 K) and 0.044 (170 K) for (II).

of imidazole 2 in the $I4_1/a$ structure. Likewise imidazoles 3 and 4 of the $P4_2/n$ structure should in principle be replaced by pairs of half-occupancy imidazoles. Instead we rely on rigid-body atomic displacement parameters to indicate what is going on.

Columns of imidazoles attached to *M*1 parallel to the **c** direction are propagated by 4_1 and 4_3 screw axes. The inversion centers within the cavities containing eight imidazoles obviously apply almost exactly in the ordered cavity model for imidazoles 3 and 4, blocking communication between columns of imidazoles attached to *M*1 parallel to the **c** direction in the $P4_2/n$ structure. The ability to switch between the inversion-related environments of a cavity only exists above the transition temperature and the requirements to become ordered in the space group $I4_1/a$ are revealed by studying the $P4_2/n$ structure just above the transition point.

3.3. Description of the *P*2/*n* phase

The ordering of the disordered $P4_2/n$ structure to create a $P2/n$ structure allows the lost 4_2 symmetry operation to create twinned components related by a 90° rotation about the monoclinic axis. Imidazoles 1–8 of the $P2/n$ asymmetric unit correspond to imidazoles 1*a*, 2*b*, 3, 4, 1*b*, 2*a*, 3, 4 of the $P4_2/n$ asymmetric unit. Rings 1–4 are obtained by the transformation $x = x_p$, $y = z_p$, $z = y_p$ and imidazoles 5–8 are obtained by a further transformation $x' = -z + 1$, $y' = y - \frac{1}{2}$, $z' = x + \frac{1}{2}$. Imidazoles 1–4 and their inversion equivalents create a centrosymmetric cavity in which all eight imidazoles are involved in hydrogen bonding, whereas imidazoles 5–8 and their inversion equivalents create a centrosymmetric cavity in which only six imidazoles are involved in hydrogen bonding. Imidazole 6 is not used for hydrogen bonding. Figs. 4(*a*) and (*b*) show the hydrogen bonds about the inversion centers at 0, 1, $\frac{1}{2}$ and $\frac{1}{2}, \frac{1}{2}, \frac{1}{2}$. The angles between the normals to the imidazole planes for rings 5–8 and rings 1–4 transformed by the pseudo-symmetry operation $-z + 1, y - \frac{1}{2}, x + \frac{1}{2}$ are 48.0 (1, 5), 71.3 (2, 6), 1.4 (3, 7) and 13.6° (4, 8) at 100 K.

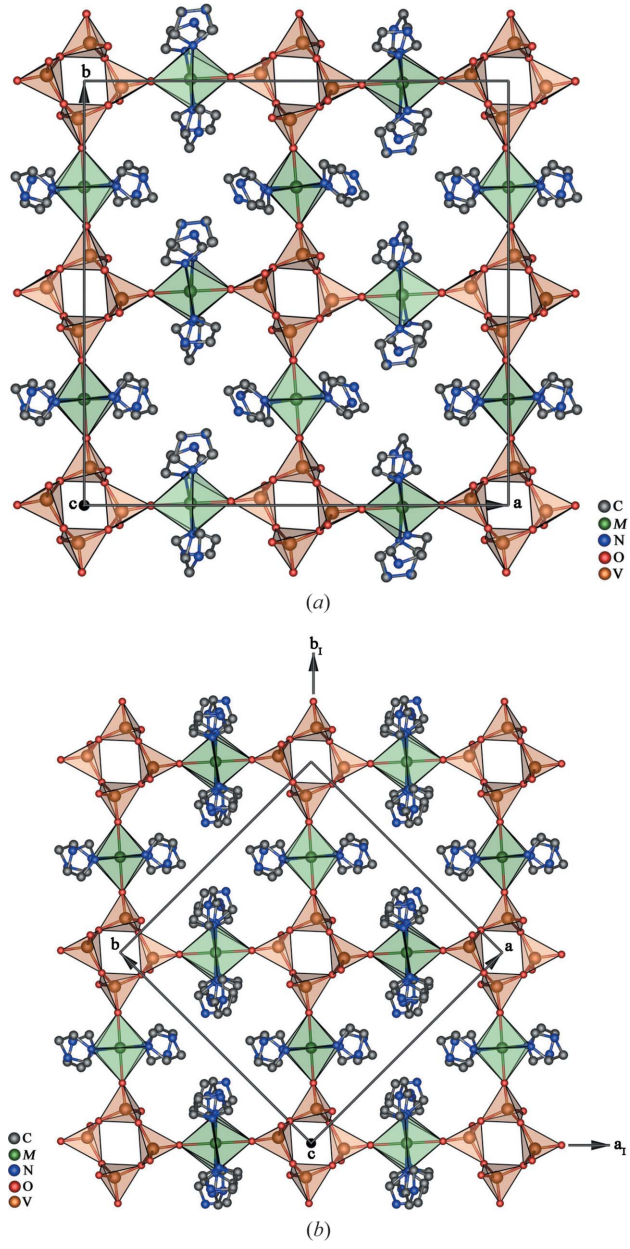

Figure 2
Polyhedral representation of single layers of the title compounds (*a*) $I4_1/a$ at $z = \frac{1}{2}$ and (*b*) $P4_2/n$ at $z = 1$, viewed along the crystallographic **c** axis.

Table 5
Largest principal libration values for the imidazoles of the low-temperature phase [$I4_1/a$ for (I), (II) and $P2/n$ for (III)].

Imidazole ring	Libration tensor (rad^2)					
	(I) at 100 K	(I) at 200 K	(I) at 279 K	(II) at 100 K	(II) at 170 K	(III) at 100 K
1	0.0009 (3)	0.004 (1)	0.0105 (3)	0.0046 (9)	0.007 (1)	0.009 (1)
2	0.025 (1)	0.030 (1)	0.0437 (4)	0.034 (1)	0.039 (2)	0.034 (1)
3	0.0016 (1)	0.0026 (1)	0.0050 (1)	0.0026 (5)	0.0044 (6)	0.0009 (1)
4	0.0092 (8)	0.017 (1)	0.0254 (4)	0.0060 (7)	0.0033 (4)	0.0046 (7)
5	0.018 (1)	0.026 (1)	0.0354 (6)	0.024 (1)	0.029 (2)	0.0055 (9)
6	0.023 (1)	0.044 (4)	0.0700 (1)	0.034 (1)	0.053 (3)	0.012 (1)
7	0.0044 (6)	0.006 (1)	0.0110 (2)	0.0040 (6)	0.008 (1)	0.0002 (5)
8	0.0053 (7)	0.010 (1)	0.0263 (5)	0.0127 (1)	0.051 (3)	0.0007 (1)

Table 6
Largest principal libration values for the imidazoles of the high-temperature phase.

Imidazole ring	Libration tensor (rad^2)				
	(I) at 283 K	(I) at 295 K	(II) at 180 K	(II) at 295 K	(III) at 295 K
1*b*	0.025 (3)	0.018 (3)	0.015 (2)	0.013 (2)	0.012 (2)
2*a*	0.016 (3)	0.031 (4)	0.0621 (3)	0.071 (4)	0.101 (4)
3	0.014 (2)	0.015 (2)	0.009 (1)	0.015 (1)	0.013 (1)
4	0.286 (7)	0.102 (3)	0.0330 (1)	0.035 (2)	0.030 (1)
1*a*	0.050 (5)	0.050 (4)	0.041 (2)	0.024 (2)	0.027 (1)
2*b*	0.122 (7)	0.147 (6)	0.206 (6)	0.291 (9)	0.254 (8)
3	0.014 (2)	0.015 (2)	0.009 (1)	0.015 (1)	0.013 (1)
4	0.286 (7)	0.102 (3)	0.0330 (1)	0.035 (2)	0.030 (1)

Table 7
Departure from equivalence of pseudo-symmetry-related imidazoles for the low-temperature phase [$I4_1/a$ for (I), (II) and $P2/n$ for (III)].

Imidazole ring		Angle between normals to planes (°)					
		(I) at 100 K	(I) at 200 K	(I) at 279 K	II at 100 K	(II) at 170 K	(III) at 100 K
1	5	25.0	24.2	22.9	25.6	25.3	48.0
2	6	127.6	129.0	130.1	124.5	124.2	71.3
3	7	3.1	3.1	2.7	2.4	2.2	1.4
4	8	52.8	53.4	52.4	55.5	55.1	13.6

Table 8
Departure from equivalence of pseudo-symmetry-related imidazoles for the high-temperature phase.

Imidazole ring		Angle between normals to planes (°)				
		(I) at 283 K	(I) at 295 K	(II) at 180 K	(II) at 295 K	(III) at 295 K
1*a*	1*b*	23.6	23.0	29.8	23.1	34.9
2*a*	2*b*	122.6	114.1	108.0	109.5	109.8
3	3	14.0†	14.0†	11.0†	14.0†	13.1†
4	4	59.2†	36.7†	20.8†	21.4†	19.7†

† Evaluated as $2(L_{ii})^{1/2}$, see text.

3.4. Change of structure with temperature

The cell dimensions for each temperature are given in Tables 1–3. Although the unit-cell volume decreases with a decrease in temperature [(I), V = 3962.7 (1) Å^3 at 295 K, 3953.4 (1) Å^3 at 283 K, $V/4$ = 3948.5 (1) Å^3 at 279 K, 3937.6 (1) Å^3 at 200 K, 3926.7 (1) Å^3 at 100 K; (II), V = 3864.7 (1) Å^3 at 295 K, 3845.04 (9) Å^3 at 180 K, $V/4$ = 3832.8 (1) Å^3 at 170 K, 3823.6 (1) Å^3 at 100 (2) K; (III), V = 3820.27 Å^3 at 295 K and 3788.63 (1) Å^3 at 100 K], the **c** axis actually increases sharply near the $P4_2/n$ to $I4_1/a$ transition temperature when approached from above [(I), c = 14.8030 (2) Å at 295 K, 14.8304 (2) Å at 283 K, $c/2$ = 14.8448 (2) Å at 279 (2) K, 14.8261 (2) Å at 200 K, 14.8002 (2) Å; (II), 14.6057 (2) Å^3 at 295 K, 14.5532 (2) Å^3 at 180 K, $c/2$ = 14.6350 (2) Å at 170 K, 14.6329 (2) Å at 100 K; (III), 14.5589 (2) Å^3 at 295 K, 14.3657 (2) Å at 100 K]. It should be pointed out that the transition temperature for the Co structure was not as well defined as for the Mn structure, presumably because the smaller unit cell for the Co structures causes what may be described as a '*sticking gate effect*'. The low-temperature Co structure persists above the transition temperature if the unit cell is determined within 10 min and the high-temperature structure has similar persistence below the transition temperature. Indeed the low-temperature Co structure was shown to have stacking faults requiring the use of two scale constants, K_1 for l even and K_2 for l odd, where K_2/K_1 = 0.819 (4) at 100 K and 0.653 (5) at 170 K. No such adjustments to the low-temperature Mn structure (I) was necessary. The 170 K structure of Co (II) is not as good as the other refinements and one suspects that K_2 may have been varying with time during data collection. Residual peaks on the heavy atoms, most noticeable when a single scale is used, persist to a lesser extent for the 170 K structure but not the 100 K structure.

The largest principal values of the libration tensor in rad^2 for each imidazole ring are given in Tables 5 and 6, using the labelling of the $I4_1/a$ structure. Tables 7 and 8 give the departure from equivalence of the imidazole rings using the difference in degrees between the directions of the normals to the planes of the imidazoles after one of each pair of rings has been transformed by a twofold rotation about a pseudo-twofold axis parallel to **c** so as to create pseudo-superposition. The structures obtained above the transition temperature have rings (3, 7) and rings (4, 8) exactly equivalent, but with a substantial libration about the relevant M—N bond. The entries in Table 8 marked (†) are obtained by evaluating

$2(L_{ii})^{1/2}$, where L_{ii} is the largest principal value of the libration tensor in rad^2, and then converting to degrees. By comparing libration parameters above and below the transition temperatures it is reasonable to assume the libration for imidazoles (3, 7) does not come from a disorder.

It is to be noted that the imidazole rings have effectively no change in their pseudo-equivalence except for rings 4 and 8, where the increase in libration with lowering temperature above the transition for the Mn structure (I) is worthy of note. The amount rings have to move to invert the environment of a pseudo-inversion center is given by the values in Tables 5 and 6 implying a big change for rings 2 and 6. As can be seen in Fig. 1(*a*), a rotation of ring 6 by $\sim 130^\circ$ to take up the alternative position must involve rotating ring 8 out of the way while maintaining its hydrogen-bond connection. Looking at (I) at 283 K (Table 6) the major libration parameter for rings (4, 8) is very similar to the value expected for a 1:1 disorder of the 279 K structure (Table 5). The smaller libration parameter at 295 K could suggest that the distribution of rings 4 and 8 is less bimodal and more Gaussian, reducing the mean square

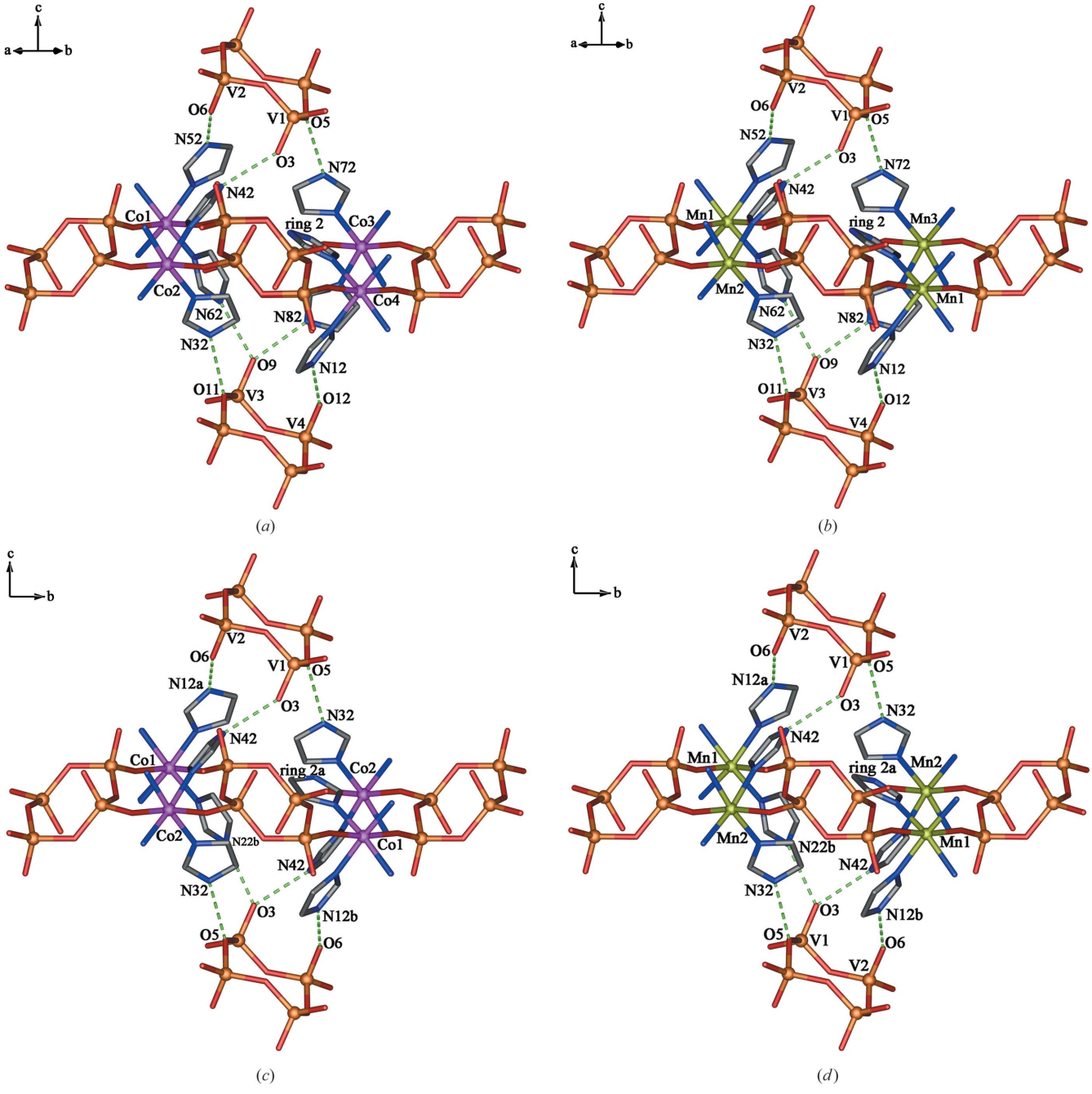

Figure 3
Hydrogen bonds about the pseudo-inversion centers $\frac{3}{4}, \frac{1}{4}, \frac{1}{2}$ for the $I4_1/a$ structure at 100 K (*a*), (*b*), and $0, \frac{1}{2}, 1$ for the $P4_2/n$ structure at 295 K (*c*), (*d*). The cobalt structure (I) is in the left column and the Mn structure (II) is in the right column. The 1:1 disorder of the $P4_2/n$ structure is not shown.

displacement. This suggests that at 283 K reasonably sized domains are already ordered in the space group $I4_1/a$. The increase in the **c** axis as the temperature is lowered above the transition temperature facilitates the transition from disorder to order. It is to be noted that in (II) the libration of ring 8 in the 295 and 180 K structures is much smaller suggesting this gate is usually stuck in a near-closed position. Things are only a bit better at 170 K, the libration increasing with the increase in the interlayer repeat. This suggests the transition temperature for (II) is nearer 170 than 180 K.

When the same approach is applied to (III), there is clear evidence that (see Tables 5–8) imidazoles 1 and 5 and not imidazoles 4 and 8 are associated with the phase transition that changes the hydrogen bonding of imidazoles 2 and 6. It is reasonable to surmise that the mechanism for ordering that pushes imidazoles 4 and 8 out of the way to allow imidazoles 2 and 6 to switch hydrogen-bonding arrangements has been closed down because of the smaller Ni atom, and replaced by an alternative mechanism that involves a monoclinic distortion of the unit cell and the creation of alternate layers of different hydrogen bonding. As seen from Figs. 4(*a*) and (*b*) the extra hydrogen bonds in Fig. 4(*a*) compared with Fig. 4(*b*) make the *c* axis of 16.3422 (2) Å longer than the *a* axis of 16.1379 (2) Å. The distortion is not present in the high-

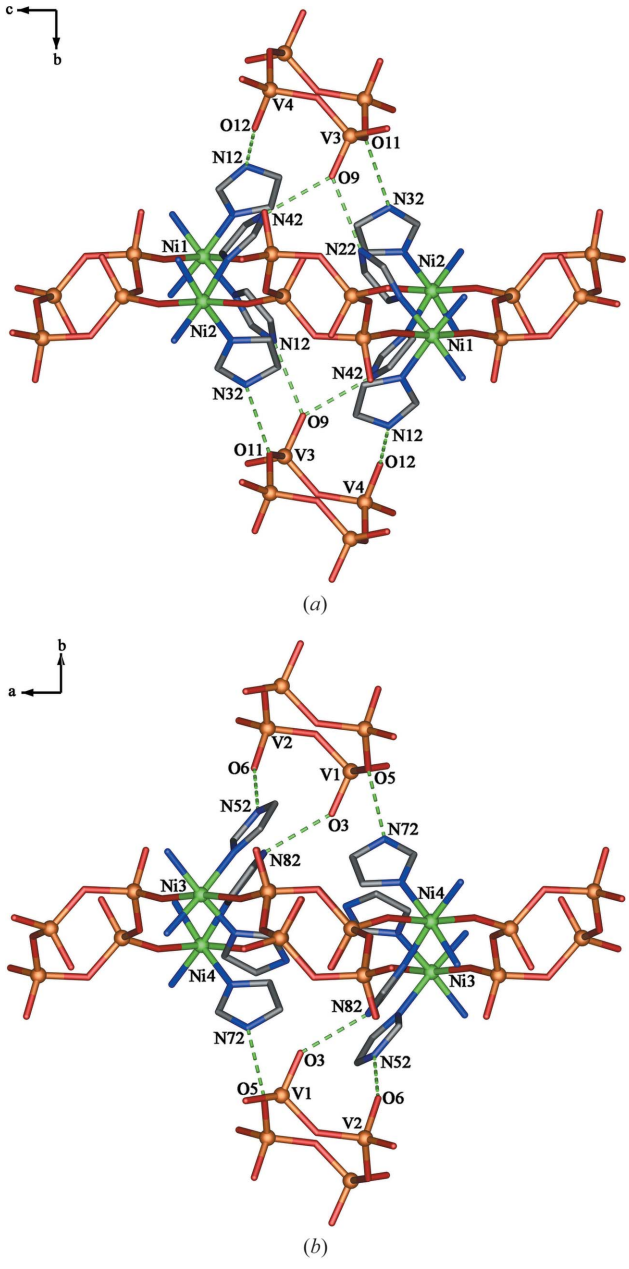

Figure 4
Hydrogen bonds about the inversion centers at (*a*) 0, 1, $\frac{1}{2}$, and (*b*) $\frac{1}{2}$, $\frac{1}{2}$, $\frac{1}{2}$ for the ordered *P*2/*n* structure of (III) at 100 K. The *c* axis is horizontal in (*a*) and the *a* axis is horizontal in (*b*).

Table 9
Selected bond lengths (Å) of (I), and (II) at 100 K.

	(I), Mn	(II), Co
*M*1—N11	2.262 (1)	2.143 (1)
*M*1—N21*a*	2.260 (1)	2.138 (2)
*M*1—N21*b*	2.260 (1)	2.138 (2)
*M*1—N51	2.262 (1)	2.139 (1)
*M*1—N61	2.216 (1)	2.109 (1)
*M*2—N31	2.264 (1)	2.156 (1)
*M*2—N41	2.252 (1)	2.130 (1)
*M*3—N71	2.257 (1)	2.147 (1)
*M*3—N81	2.246 (1)	2.131 (1)
*M*1—O1	2.157 (1)	2.112 (2)
*M*1—O7	2.202 (1)	2.140 (2)
*M*2—O4	2.132 (1)	2.075 (2)
*M*3—O10	2.126 (1)	2.074 (2)
V1—O1	1.651 (1)	1.650 (2)
V1—O2	1.796 (1)	1.798 (2)
V1—O3	1.637 (1)	1.641 (2)
V1—O5	1.820 (1)	1.827 (2)
V2—O2^{i}	1.804 (1)	1.811 (2)
V2—O4	1.644 (1)	1.643 (2)
V2—O5	1.812 (1)	1.809 (2)
V2—O6	1.638 (1)	1.642 (2)
V3—O7	1.640 (1)	1.635 (2)
V3—O8	1.796 (1)	1.798 (2)
V3—O9	1.650 (1)	1.653 (2)
V3—O11	1.810 (1)	1.817 (2)
V4—O8^{ii}	1.806 (1)	1.810 (2)
V4—O10	1.641 (1)	1.642 (2)
V4—O11	1.814 (1)	1.814 (2)
V4—O12	1.633 (1)	1.637 (2)

Symmetry codes: (i) $-x+2, -y+1, -z+1$; (ii) $-x+1, -y+1, -z+1$.

Table 10
Selected bond lengths (Å) of (III) at 100 K.

Ni1—N11	2.062 (1)	V1—O3	1.643 (2)
Ni1—N21	2.057 (1)	V1—O5	1.831 (2)
Ni2—N31	2.100 (1)	V2—O2^{i}	1.810 (2)
Ni2—N41	2.068 (1)	V2—O4	1.649 (2)
Ni3—N51	2.085 (1)	V2—O5	1.820 (2)
Ni3—N61	2.055 (2)	V2—O6	1.641 (2)
Ni4—N71	2.102 (1)	V3—O7	1.646 (2)
Ni4—N81	2.080 (1)	V3—O8	1.798 (2)
Ni1—O1	2.111 (2)	V3—O9	1.649 (2)
Ni2—O4	2.057 (2)	V3—O11	1.823 (2)
Ni3—O7	2.121 (2)	V4—O8^{ii}	1.818 (2)
Ni4—O10	2.077 (2)	V4—O10	1.650 (2)
V1—O1	1.651 (2)	V4—O11	1.821 (2)
V1—O2	1.809 (2)	V4—O12	1.630 (2)

Symmetry codes: (i) $-x+1, -y+2, -z+1$; (ii) $-x+1, -y+1, -z+2$.

Table 11
Hydrogen-bond geometry (Å, °) for (I) and (II) at 100 and 295 K.

Hydrogen-bond geometry at other temperatures [200, 279, 283 K for (I) and 170, 180 K for (II)] is given in the deposited CIF.

			H···A		D···A		∠ D—H···A	
T (K)	D—H···A	D—H	(I)	(II)	(I)	(II)	(I)	(II)
100	N12—H1N12···O12^{i}	0.86	1.97	1.96	2.774 (2)	2.754 (2)	163	154
100	N32—H1N32···O11^{ii}	0.86	2.07	2.12	2.890 (2)	2.912 (2)	159	154
100	N42—H1N42···O3^{iii}	0.86	2.00	2.00	2.791 (2)	2.775 (2)	153	149
100	N52—H1N52···O6^{i}	0.86	1.96	1.93	2.782 (2)	2.757 (2)	161	162
100	N62—H1N62···O9^{iii}	0.86	2.02	2.04	2.851 (2)	2.853 (2)	161	157
100	N72—H1N72···O5^{iv}	0.86	1.99	2.05	2.764 (2)	2.796 (2)	149	145
100	N82—H1N82···O9^{iii}	0.86	1.92	1.91	2.762 (2)	2.758 (2)	166	167
295	N12*b*—H1N12*b*···O6^{v}	0.86	1.96	1.99	2.797 (4)	2.808 (5)	165	160
295	N22*b*—H1N22*b*···O3^{vi}	0.86	2.03	2.02	2.875 (3)	2.860 (4)	167	166
295	N32—H1N32···O5^{vii}	0.86	2.07	2.07	2.871 (2)	2.865 (3)	154	154
295	N42—H1N42···O3^{vi}	0.86	1.97	1.93	2.773 (3)	2.763 (3)	155	162

Symmetry codes: (i) $-y+\frac{5}{4}, x-\frac{1}{4}, z-\frac{1}{4}$; (ii) $y+\frac{1}{4}, -x+\frac{3}{4}, -z+\frac{3}{4}$; (iii) $y+\frac{1}{4}, -x+\frac{5}{4}, z+\frac{1}{4}$; (iv) $y+\frac{1}{4}, -x+\frac{7}{4}, -z+\frac{3}{4}$; (v) $y-\frac{1}{2}, -x+1, z-\frac{1}{2}$; (vi) $y-\frac{1}{2}, -x+1, z+\frac{1}{2}$; (vii) $-y+\frac{1}{2}, x, -z+\frac{3}{2}$.

Table 12
Hydrogen-bond geometry (Å, °) for (III) at 100 and 295 K.

T (K)	D—H···A	D—H	H···A	D···A	∠ D—H···A
100	N12—H1N12···O12^{i}	0.86	1.98	2.732 (2)	145.7
100	N22—H1N22···O9^{ii}	0.86	2.10	2.893 (2)	152.9
100	N32—H1N32···O11^{iii}	0.86	2.21	2.950 (2)	144.0
100	N42—H1N42···O9^{iii}	0.86	1.94	2.743 (2)	154.5
100	N52—H1N52···O6^{iv}	0.86	1.90	2.716 (2)	159.0
100	N72—H1N72···O5^{v}	0.86	2.03	2.815 (2)	151.1
100	N82—H1N82···O3	0.86	2.13	2.829 (2)	137.9
295	N12*a*—H1N12*a*···O6^{vi}	0.86	1.92	2.722 (3)	154.0
295	N12*b*—H1N12*b*···O6^{vi}	0.86	1.92	2.757 (3)	163.8
295	N22*b*—H1N22*b*···O3^{vii}	0.86	2.10	2.924 (2)	159.7
295	N32—H1N32···O5^{viii}	0.86	2.15	2.913 (2)	147.7
295	N42—H1N42···O3^{vii}	0.86	2.00	2.771 (2)	148.7

Symmetry codes: (i) $-x+\frac{1}{2}, y, -z+\frac{3}{2}$; (ii) $-x+\frac{1}{2}, y+1, -z+\frac{3}{2}$; (iii) $x-\frac{1}{2}, -y+1, z-\frac{1}{2}$; (iv) $x, y-1, z$; (v) $-x+1, -y+1, -z+1$; (vi) $y-\frac{1}{2}, -x+1, z-\frac{1}{2}$; (vii) $y-\frac{1}{2}, -x+1, z+\frac{1}{2}$; (viii) $-y+\frac{1}{2}, x, -z+\frac{3}{2}$.

temperature form of (III) and suggests that all cavities contain seven hydrogen-bonded imidazoles for the $P4_2/n$ structures.

3.5. Bond lengths and angles

Bond lengths are in remarkably good agreement over the whole temperature range and are most reliable for the 100 K structures in space group $I4_1/a$. The Mn–N distances range from 2.216 (1) to 2.264 (1) Å, mean 2.253 Å, and the Mn—O distances range from 2.126 (1) to 2.202 (1) Å, mean 2.154 Å. If the Mn1—N21 bond is omitted since this imidazole is disordered, then the Mn—N range is 2.216 (1)–2.264 (1) Å, mean 2.251 Å. These are slightly longer than the bond lengths for Co and Ni, namely, Co—N distances range from 2.109 (1) to 2.156 (1) Å, mean 2.137 Å, and the Co—O distances range from 2.074 (2) to 2.140 (2) Å, mean 2.100 Å. If the Co1—N21 bond is omitted, then the Co—N range is 2.057 (1) to 2.100 (1) Å, mean 2.076 Å. The Ni—N distances range from 2.109 (1) to 2.156 (1) Å, mean 2.137 Å, and the Ni—O distances range from 2.074 (2) to 2.140 (2) Å, mean 2.100 Å. However, it should be noted that the imidazole not involved in hydrogen bonding always had the shortest *M*—N bond in all refinements. The bond lengths around V fall into three groups:

(i) those involving O atoms bridging (μ_2-O) vanadium atoms,

(ii) those involving O atoms bridging (μ_2-O) a vanadium and an *M* atom, and

(iii) those involving terminal O atoms.

For the Mn structure V—O distances:

(i) vary from 1.796 (1) to 1.820 (1) Å, mean 1.807 Å, V—O distances;

(ii) vary from 1.640 (1) to 1.651 (1) Å, mean 1.644 Å, and V—O distances;

(iii) vary from 1.633 (1) to 1.650 (1) Å, mean 1.640 Å.

For the Co structure, V—O distances:

(i) vary from 1.798 (1) to 1.827 (1) Å, mean 1.811 Å, V—O distances;

(ii) vary from 1.635 (2) to 1.650 (2) Å, mean 1.643 Å, and V—O distances;

(iii) vary from 1.637 (1) to 1.653 (1) Å, mean 1.643 Å.

For the Ni structure, V—O distances:

(i) vary from 1.798 (2) to 1.831 (2) Å, mean 1.816 Å, V—O distances;

(ii) vary from 1.640 (2) to 1.651 (2) Å, mean 1.649 Å, and V—O distances;

(iii) vary from 1.630 (1) to 1.649 (1) Å, mean 1.641 Å.

The O—V—O bond angles range from 107.3 (1) to 112.9 (1)°, mean value 109.5° for Mn, from 107.3 (1) to 113.0 (1)°, mean value 109.5° for Co, and from 107.4 (1) to 111.5 (1)°, mean value 109.5° for Ni. It is seen that the tetrahedral angles around V correspond to the ideal value of 109.5°.

4. Conclusions

The different order–disorder phase transition behaviors in the three isomorphous polymers of the type $[M(\mathrm{Im})_4\mathrm{V_2O_6}]_\infty$ on cooling can be attributed to a decrease in *M*—N and *M*—O bond lengths for the sequence Mn > Co > Ni. At 295 K, all crystals are 1:1 disordered in the space group $P4_2/n$ (Z = 8),

and are reversibly transformed to an ordered $I4_1/a$ ($Z = 32$) or $P2/n$ ($Z = 8$) phase at 100 K for Mn and Co, or Ni. As the M atom becomes smaller, an easy mechanism for ordering (Mn) becomes more difficult (Co), and then impossible (Ni). The Ni complex finds a new and different ordered structure in the space group $P2/n$.

KC would like to thank The Australian Government Department of Education, Science and Training (DEST) for financial support under the 2006 Endeavour Asia Awards.

References

Altomare, A., Burla, M. C., Camalli, M., Cascarano, G. L., Giacovazzo, C., Guagliardi, A., Moliterni, A. G. G., Polidori, G. & Spagna, R. (1999). *J. Appl. Cryst.* **32**, 115–119.

Blessing, R. H. (1995). *Acta Cryst.* A**51**, 33–38.

Brandenburg, K. & Putz, H. (2006). *DIAMOND*, Version 3.1e. Crystal Impact GbR, Bonn, Germany.

Brese, N. E. & O'Keeffe, M. (1991). *Acta Cryst.* B**47**, 192–197.

Brown, I. D. & Altermatt, D. (1985). *Acta Cryst.* B**41**, 244–247.

Burnett, M. N. & Johnson, C. K. (1996). *ORTEP*III. Report ORNL-6895. Oak Ridge National Laboratory, Tennessee, USA.

Cheetham, A. K., Férey, G. & Loiseau, T. (1999). *Angew. Chem. Int. Ed. Engl.* **38**, 3268–3292.

Chesnut, D. J., Hagrman, D., Zapf, P. J., Hammond, R. P., LaDuca, R., Haushalter, R. C. & Zubieta, J. (1999). *Coord. Chem. Rev.* **190–192**, 737–769.

Chirayil, T., Zavalij, P. Y. & Whittingham, M. S. (1998). *Chem. Mater.* **10**, 2629–2640.

Creagh, D. C. & McAuley, W. J. (1995). *International Tables for X-ray Crystallography*, edited by A. J. C. Wilson, Vol. C, Table 4.2.6.8, pp. 219–222. Dordrecht: Kluwer Academic Publishers.

Fuchs, J., Mahjour, S. & Pickardt, J. (1976). *Angew. Chem. Int. Ed. Engl.* **15**, 374–375.

Hahn, Th. (1995*a*). Editor. *International Tables for X-ray Crystallography*, Vol. A. pp. 344–345. Dordrecht: Kluwer Academic Publishers.

Hahn, Th. (1995*b*). Editor. *International Tables for X-ray Crystallography*, Vol. A. pp. 350–351. Dordrecht: Kluwer Academic Publishers.

Hagrman, P. J., Finn, R. C. & Zubieta, J. (2001). *Solid State Sci.* **3**, 745–774.

Herbstein, F. H. (2006). *Acta Cryst.* B**62**, 341–383.

Höwing, J., Gustafsson, T. & Thomas, J. O. (2003). *Acta Cryst.* B**59**, 747–752.

Krachodnok, S., Haller, K. J. & Williams, I. D. (2008). *Adv. Mater. Res.* **55–57**, 669–672.

Law, T. S.-C., Sung, H. H.-Y. & Williams, I. D. (2000). *Inorg. Chem. Commun.* **3**, 420–423.

Law, T. S.-C. & Williams, I. D. (2000). *Chem. Mater.* **12**, 2070–2072.

Lin, X., Telepeni, I., Blake, A. J., Dailly, A., Brown, C. M., Simmons, J. M., Zoppi, M., Walker, G. S., Thomas, K. M., Mays, T. J., Hubberstey, P., Champness, N. R. & Schröder, M. (2009). *J. Am. Chem. Soc.* **131**, 2159–2171.

Maspoch, D., Ruiz-Molina, D. & Veciana, J. (2007). *Chem. Soc. Rev.* **36**, 770–818.

Natarajan, S. & Mandal, S. (2008). *Angew. Chem. Int. Ed. Engl.* **47**, 4798–4828.

Nonius (1998). *COLLECT*. Nonius BV, Delft, The Netherlands.

O'Keeffe, M., Peskov, M. A., Ramsden, S. J. & Yaghi, O. M. (2008). *Acc. Chem. Res.* **41**, 1782–1789.

Otwinowski, Z. & Minor, W. (1997). *Methods in Enzymology*, Vol. 276, *Macromolecular Crystallography*, Part A, edited by C. W. Carter Jr & R. M. Sweet, pp. 307–326. New York: Academic Press.

Oxford Cryosystems (1997). *600 Series Cryostream Cooler Operation and Instruction Guide.* Oxford Cryosystems, Oxford, UK.

Rae, A. D. (1975*a*). *Acta Cryst.* A**31**, 560–570.

Rae, A. D. (1975*b*). *Acta Cryst.* A**31**, 570–574.

Rae, A. D. (2006). *RAELS*06. Australian National University, Canberra, Australia.

Sharma, S., Ramanan, A., Zavalij, P. Y. & Whittingham, M. S. (2002). *CrystEngComm*, **40**, 601–604.

Whittingham, M. S. (2004). *Chem. Rev.* **104**, 4271–4302.

Williams, I. D., Law, T. S.-C., Sung, H. H.-Y., Wen, G.-H. & Zhang, X.-X. (2000). *Solid State Sci.* **2**, 47–55.

Xie, Z., Ma, L., deKrafft, K. E., Jin, A. & Lin, W. (2010). *J. Am. Chem. Soc.* **132**, 922–923.

Zavalij, P. Y. & Whittingham, M. S. (1999). *Acta Cryst.* B**55**, 627–663.